DESIGN AND THERMAL ANALYSIS OF IMPULSE THRUSTERS FOR CONTROL SYSTEMS OF GUIDED MISSILES

by

Toufik ALLOUCHE[a*], Saša Ž. ŽIVKOVIĆ[b], Abdellah FERFOURI[a], Damir D. JERKOVIĆ[a], Nebojša P. HRISTOV[a] and Marko Z. KARIĆ[b]

[a] University of Defence – Military Academy, Belgrade, Serbia

[b] Military Technical Institute, Belgrade, Serbia

[*]Corresponding author; E-mail: toufik.allouche@gmail.com

This paper presents design analysis of impulse thrusters intended for guidance and control systems of missiles. Impulse thrusters are small solid propellant, short-operation, high thrust rocket motors. They are mounted laterally on the missile's control block, and are used to generate control forces to adjust its trajectory. To minimize the control block weight and achieve better missile performances, aluminum alloy is utilized, due to its favorable strength-to-weight ratio and ease of manufacturing productivity. However, the sensitivity of aluminum alloys to high temperatures necessitates a comprehensive thermal analysis, to ensure structural integrity and performance reliability under operational conditions. For that, three impulse thruster models are designed with incrementally higher thrust and thermal loading. An internal ballistic model is employed to predict their performances, with results validated through static experimental tests. Then, numerical CFD and heat transfer simulations are conducted, to predict eventual thruster block structure overheating, to achieve the maximum possible performances. The study highlights the importance of material selection, thermal analysis, and propellant design for optimizing impulse thruster performance and ensuring the reliability of control systems of missiles.

Key words*: Impulse thruster, control block, heat transfer, internal ballistic static tests.*

1. Introduction

In modern defense technology, missile control systems are one of the most important cornerstones as they provide guidance, precision and stabilization of missiles under external disturbances during flight. Missile control systems fall into three main categories [1, 2]: aerodynamic control systems, thrust vectoring and reaction control – impulse thrusters. The last ones are small solid propellant, short-operation time, high-force rocket motors (RMs), mounted in the lateral side of the missile, intended to generate a force able to change the missile's direction to adjust its trajectory [3].

Control systems based on thrusters, do not have widespread applications even though are particularly advantageous, as they offer: faster response time, so they can enhance maneuverability [4]

and agility at various angles of attack, missile velocities and altitudes [5]; system simplicity and reliability; higher precision of control force generating; better mass performances; less power consumption, while adhering to the current trend of minimizing production costs [6], making them versatile to different missions.

Thanks to their characteristics, control method based on impulse thrusters has been integrated into several areas including: spacecraft engineering, satellite technology, rocket and missile systems. In missile technology, thrusters are used for various functions, especially in applications requiring fast and precise adjustments, such as artillery, anti-ballistic and air defense missiles, and anti-tank missiles.

In artillery, impulse thrusters can improve the accuracy of unguided rockets by enabling precise trajectory correction. For example, rocket R624 of the multiple launch rocket system WILCHA (fig.1(a) left), on the front part of the rocket is implemented a control block composed of 90 thrusters, arranged around the guidance section [7]. In air defense, impulse thrusters are used to increase maneuverability and to refine the course of missiles in terminal phase of flight. The PAC-3 missile used in the air defense system PATRIOT, is equipped with 180 side mounted thrusters to ensure higher precision. One of rare applications in anti-tank missiles is the M-47 DRAGON, which contains a control system composed of 60 thrusters installed on the side surface of the missile. They have an inclination of 40 degrees relative to the rocket axis to achieve maneuverability and to sustain velocity of the missile [8].

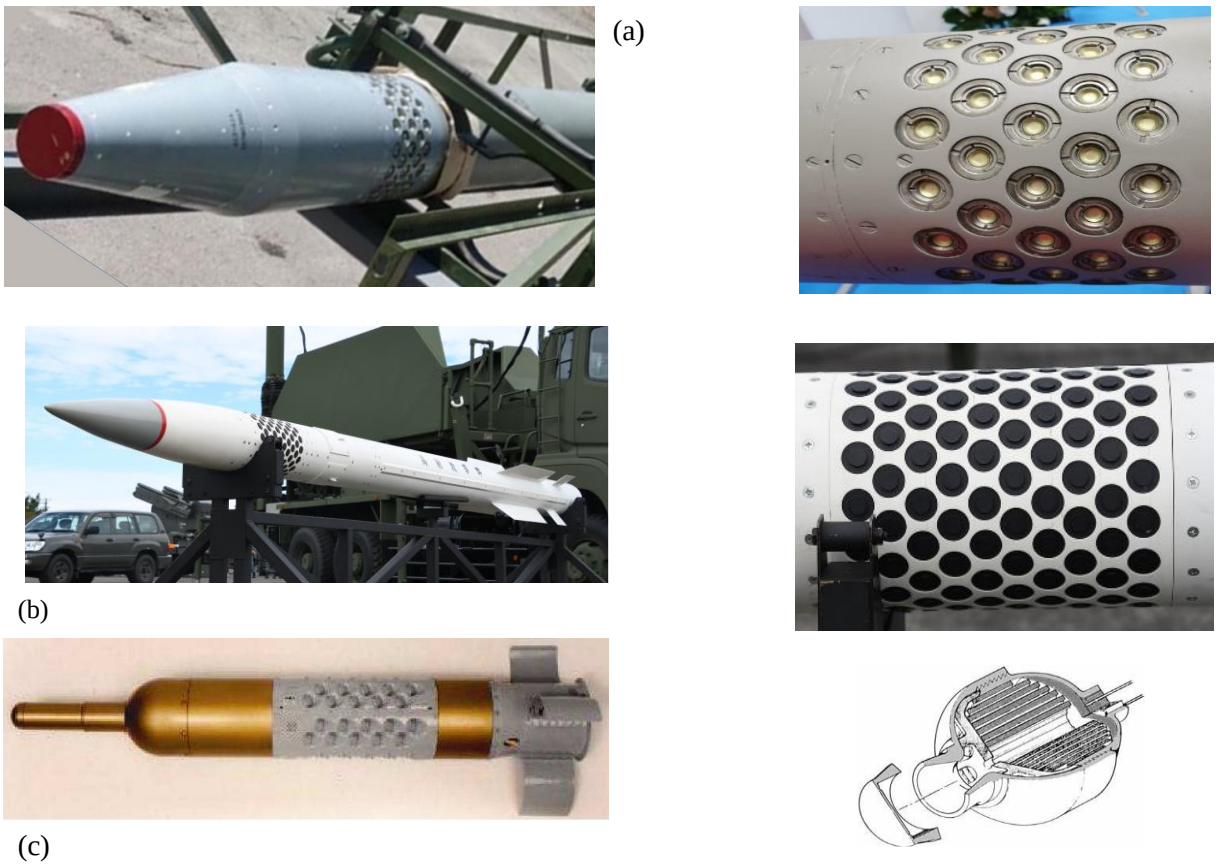

(a)

(b)

(c)

Figure 1. Missiles using lateral thrusters:
(a) R624 missile [7] (left) and R624 control section [9] (right),
(b) PAC-3 missile [10] (left) and control section of PAC-3 [11] (right),
(c) M-47 DRAGON missile [12] (left) and M-47 DRAGON'S thruster [8] (right)

Thruster operating requirements can vary widely depending on the missile's purpose and characteristics. The required operating time can range from a few to several hundred milliseconds, depending on the system's dynamics. Thrust values can also range from a few to several hundred newtons, depending on the required maneuverability and the missile size. These two parameters indirectly determine the mechanical and thermal loads on the thruster structure; as they define intensity of heat flux and exposure time of the structure, to the heat from combustion products.

One of advantages of thruster control systems is the good mass performance (less system weight compared to summary control force-time integral). During design of those systems, it is essential to optimize its size and mass to be minimum as possible, while ensuring that it can withstand the operating mechanical and thermal loads. Various design solutions for the control block with thrusters can be applied. One variant involves the use of an optimal thruster design in the form of spherical motors, which are installed using lightweight fairings (Dragon missile fig.1(c) left). If larger number of thrusters is needed, to achieve simplicity of construction and even better mass performance for the control system, in some systems a lightweight cylindrical housing with installed thrusters has been applied (fig. 1(a) right and 1(b) right). This simplifies the design and assembly of the entire system, while also reducing simultaneously mass by eliminating additional components required for connecting the motors to the missile body.

Aluminum alloys are widely used in rocket technology due to their relatively high specific strength-to-weight ratio [13] and low costs, however, they have limited resistance to thermal stress and a very high thermal conductivity coefficient, which can be a limiting factor for their use in thrusters control blocks. However, the operating parameters and material characteristics are such that, in some cases, the use of high-strength aluminum alloys is possible, which favorably impacts the mass performance of the system. Thrusters operating time is typically very short, usually falling into the category of impulse RMs. Thanks to this fact, the amount of heat transferred to the motor walls is generally very low, making it possible in certain cases, to use aluminum alloys without additional thermal insulation.

In practice, rockets often rotate around their longitudinal roll-axis. The rotation depends on the type of the rocket, and the guidance system, ranging from 0 for non-rotating-rockets to several tens of Hz for slow-rotating rockets, or up to several hundreds of Hz for fast-rotating-rockets (or gyroscopically stabilized rockets). During the operating time of the thruster, the rocket rotates by a certain angle having an impact on the resulting force. This angle depends on the spin rate and the operating time of the thruster, and must be minimal. As example, for an artillery rocket with a spin about 25 Hz, for a permissible deflection angle up to 90°, thruster operating time is about 10 ms.

To achieve the desired short operation time of the RM, it is necessary to use a propellant with a high burning rate, specific shapes of propellant grain, and high motor pressure. Certain grain configurations in Solid propellant Rocket Motors (SPRMs) offer high surface burning areas and fast burning, such as multi-perforated cylinders, multiple-tubes and spirals.

2. Thrusters design

To assess the design possibilities of a high-performance thruster block made of aluminum alloy, it is necessary to evaluate the maximum operating parameters that can be achieved in a specific configuration of the control block. For the calculations and experimental measurements of

performance, a model of a thrusters control block of artillery rocket was chosen. The RM operating time of 11 ms was specified for typical rotation of such projectiles. An operating pressure of 200 bars was chosen to achieve high burning rate for the available propellant material. In order to test the thermal resistance of the thruster block and apply high-strength aluminum alloy, the size of the thruster propellant grain was varied in a thrust range from 500 N to 1100 N.

Thrusters used in missile control systems have some specific requirements similar to impulse motors, compared to other types of RMs [12, 14], as: rapid ignition, short operating time, high burning rate propellant, high operating pressure and a compact size. To predict the impulse thruster performances, different mathematical models were proposed. The study [14] is dedicated to the design of impulse thrusters, with focus on performances, their dynamics and the high burning rate propellants. Thrusters can be designed using the RM design process, as given in the report [15], which provides an overview of SPRMs performances requirements, propellant properties, motor components, and performance equations. In [16], a method is proposed to determine realistic IB (internal ballistic) coefficients and performance parameters, including specific impulse, thrust coefficient, and discharge coefficient. These characteristic RM performance parameters are used for initial RM design, as described in [17], to determine starting parameters such as propellant mass, RM structure mass and geometry, propellant burning rate, nozzle geometry, etc.

2.1. Internal ballistic calculation

After more precise design of the propellant grain geometry [18], and the structural elements of the RM, and also after determining the burning rate law, more accurate performances can be predicted using the unsteady internal ballistic mathematical model [16]. This unsteady calculation is necessary to take into account intensely transient processes which occurs during operation of impulse RMs. The pressure-time, thrust-time and burned web-time curves can be predicted solving the system of differential equations presented as follows:

$$\frac{d}{dt}p_c(t)=\frac{R\cdot T_c\cdot A_b(t)\cdot r(p_c,t)\cdot\rho_p}{V_c(t)}-\frac{A_t}{V_c(t)}\sqrt{\kappa\cdot R\cdot T_c\left(\frac{2}{\kappa+1}\right)^{\frac{\kappa+1}{\kappa-1}}}\cdot p_c(t)-\frac{A_b(t)\cdot r(p_c,t)\cdot p_c(t)}{V_c(t)} \tag{1}$$

$$\frac{d}{dt}x(t)=r(p_c,t) \tag{2}$$

$$A_b(t)=A_b\left[x(t)\right] \tag{3}$$

$$V_c(t)=V_c(0)+\int_0^t A_b(t)\cdot r(t)dt \tag{4}$$

$$r(p_c,t)=r\left[p_c(t)\right] \tag{5}$$

$$F(t)=C_F\cdot p_c(t)\cdot A_t \tag{6}$$

In the internal ballistic calculation, the initial pressure was set to 50 bars, which represent the pressure generated by the igniter at the beginning of the combustion process, and a thrust coefficient of 1.35 was used. For more precise calculations of the change of burning surface area $A_b(x)$, it is necessary to apply numerical methods for burnback analysis [18], in order to account for complex geometry or manufacturing tolerances of the propellant grain. Burning rate law $r(p_c)$ must be obtained experimentally, to achieve satisfying accuracy.

To verify the theoretical results obtained by mathematical models, and to validate the design, it is essential to conduct experimental tests, and then compare results. To cover wide range of thrust, three models of thrusters are designed. Geometry of RM and propellant type is fixed, and also the operating pressure, which allows the design of a common combustion chamber for all models, with the possibility of installing a modular nozzle. The internal diameter of the combustion chamber is 24 mm, for a length of 13.5 mm. Initial design calculations have permitted to obtain results shown in tab. 1.

Table 1. Characteristic parameters of the three designed motors

Parameter	Value		
	Motor 1	Motor 2	Motor 3
Force [N]	500	800	1100
Operating time [s]	0.011	0.011	0.011
Internal pressure [Pa]	$200 \cdot 10^5$	$200 \cdot 10^5$	$200 \cdot 10^5$
Propellant mass [kg]	0.00272	0.00427	0.0059
Mass flow rate [kgs^{-1}]	0.2473	0.3879	0.5366
Throat diameter [m]	0.0048	0.006	0.0071
Nozzle exit diameter [m]	0.020	0.026	0.031

2.2. Propellant grain design

The selection of the propellant is one the most important processes in the RM design to achieve the required performances. It directly influences the key parameters of the RM such as: pressure and thrust - time curves, operating time, case size, etc. Thrusters are employed to deliver a short-duration impulses using fast-burn propellants with an adequate grain configuration. In this paper, only conventional double based propellant for impulse motors is considered. For the selected propellant with high burning rate, a thermochemical calculation has been performed [19]. The characteristics of the applied propellant and combustion products are provided in tab. 2. Burn rate for chosen propellant is experimentally measured [19]. Figure 2 shows burn rate of the solid propellant as a function of the combustion chamber pressure.

Table 2. Propellant characteristics

Characteristics	Value
Density [kgm^{-3}]	1620
Specific heat ratio [-]	1.24
Temperature of combustion [K]	2350
Molar mass [$kgkmol^{-1}$]	23.1
Specific impulse [$Nskg^{-1}$]	2200

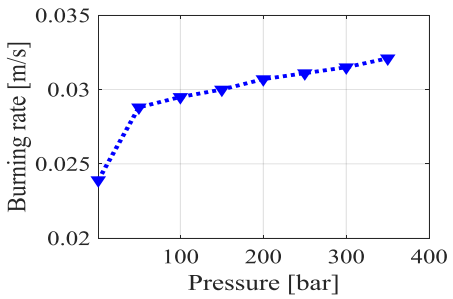

Figure 2. Burn rate as a function of pressure

The required operating time of the RM, operating pressure, and burning rate define the burning web at 0.325 mm, i.e. thickness of the propellant grain 0.65 mm. To achieve required thickness spiral tape shape grain is chosen (figure 3). The grain geometries of each motor are shown in tab. 3.

Table 3. Geometry of propellant grains

Parameter	Grain 1	Grain 2	Grain 3
Length [m]	0.191	0.3	0.415
Width [m]	0.0135	0.0135	0.0135
Thickness [m]	0.00065	0.00065	0.00065

Burning surface area calculation for a perfect (ideal) spiral-shaped grain is done by equation (7):

$$A_b(x) = 2\left[(l-2x)\cdot(L-2x)+(L-2x)\cdot(h-2x)+(l-2x)\cdot(h-2x)\right] \quad (7)$$

In fig. 3 are shown samples of the manufactured spiral-shaped propellant grains, and in fig. 4 are shown the corresponding burning surface areas relative to burned web. The ideal grain burning surface area assumes a perfectly uniform surface exposed to combustion, while the real grain burning surface area takes into consideration the imperfections introduced during manufacturing, such as dimensional tolerances and misalignments of internal features like tubes. These tolerances and geometric errors, provided by the manufacturer, are incorporated into the real grain burning surface area, which is determined through numerical burnback analysis [18]. This is important for the thrusters because, with small motor dimensions, tolerances can have a much greater impact.

Figure 3. Spiral-shaped propellant ideal geometry and manufactured samples

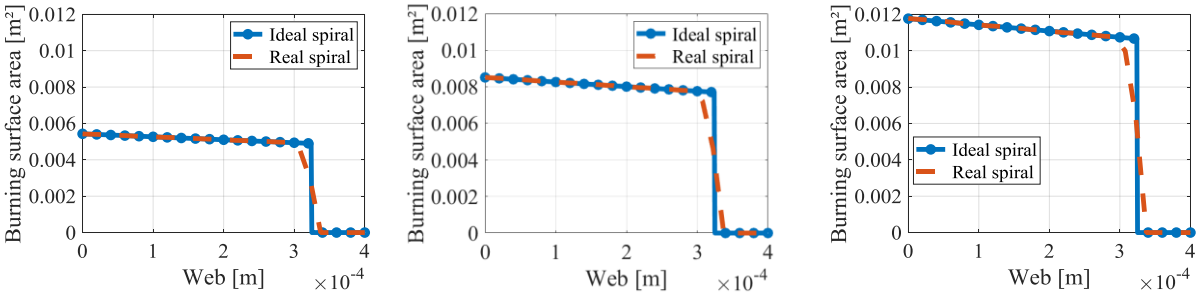

Figure 4. Burning area change of ideal and real grains: (a) Grain 1, (b) Grain 2 and (c) Grain 3

3. Static tests and results analysis

In this section, series of experimental tests are conducted. Tests consist to measure certain outputs such as combustion chamber pressure and motor thrust in time for each motor. Similar

experiment is described in [20]. The experimentation results are compared with the corresponding results predicted by calculations. These experiments fall within the scope of verification and validation of the used mathematical model for the performance prediction of solid propellant impulse thrusters.

To conduct tests, the measurement system shown in fig. 5 is used, and it consists of:

- Experimental impulse thruster rocket motor, designed with identical internal geometry, but construction is optimized to be simple for assembly, to withstand large number of tests and to enable measurement of pressure in the combustion chamber and thrust as presented in fig. 5;
- Test stand composed of a load cell (force transducer to measure the thrust) in which the thruster is mounted by means of a coupling device, and a pressure transducer connected to the chamber;
- Power: the electric device needed to generate the ignition current and the associated wiring;
- Acquisition and Processing: composed of an amplifier, an acquisition device and computer to process data and for visualization.

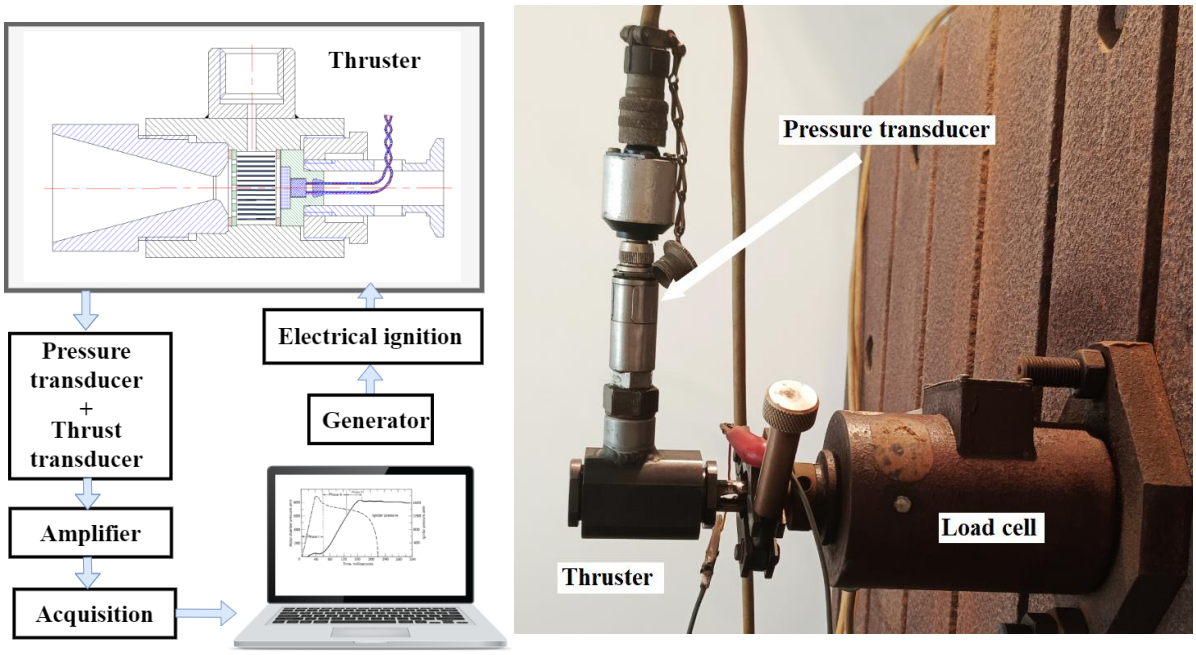

(a) (b)

Figure 5. (a) Schematic of the measurement system for static tests, (b) Test stand installation

Figure. 6 presents the predicted pressure-time and thrust-time curves, obtained by implementation of the unsteady internal ballistic mathematical model, compared with the experimentally measured results for the three motors using the propellant described in tab. 2 at an initial temperature of 20°C.

Some differences are observed between the experimental and theoretical curves. The experimental pressure and thrust curves may deviate from the theoretical ones due to transitional processes during ignition and burnout of the thruster. The typical duration of these processes is of the same order of magnitude as the effective operating time of impulse thrusters, making their influence on the overall curve shape significant. Slight deviations in thruster and propellant geometry or the ignition process, can lead to discrepancies in the experimental curves. These differences can be also attributed to measurement uncertainties, grain mass inaccuracy, grain silver remaining after combustion reaches the web, propellant fragmentation, etc. Significant curve deformations are

observed in the tests of Motors 1 and 2 as shown in fig. 6(a) and (b), while Motor 3 (Figure 6, c) exhibits a curve shape that corresponds well to the expected combustion of the propellant grain.

Generally, results demonstrate relatively good agreement in terms of values and curves shape, between the analytical predictions and the experimental data within the error margins less than 5% for pressure and thrust integral and less than 10% for effective time, as illustrated in fig. 6. This concordance validates the mathematical model used for performance predictions and confirms its applicability in the solid propellant impulse thrusters design, with considerations of the thruster's sensitivity to ignition and errors in grain geometry.

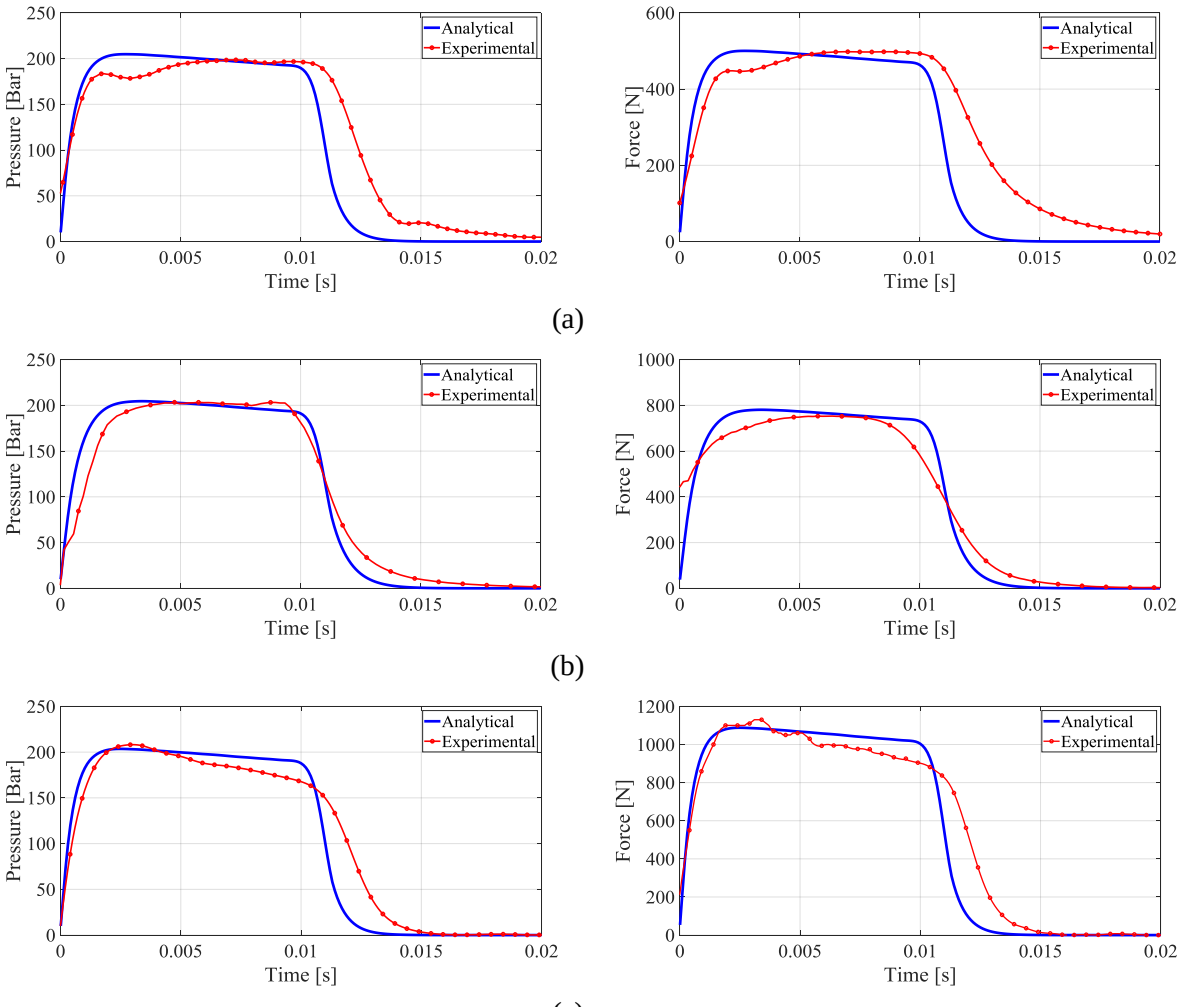

Figure 6. Analytical and experimental pressure and thrust-time curves:
(a) Motor 1, (b) Motor 2 and (c) Motor 3

4. Thermal analysis

Thrusters used in missile control systems must be light weight as possible to achieve better missile's performance. Optimization of the weight can be achieved by reduction of the case and nozzle walls thickness and by using light materials. The control block case is made of aluminum alloy 7050, or similar. Nozzle insert from high density graphite is applied in the maximal thermal loaded throat area. The objective is to design a control block section intended to house multiple thrusters, which size

must be minimal, as well as the distance separating them. Two negative effects may occur in this construction:

1. During thruster operation, the inner walls heat up, and the temperature of the inner wall layers rises significantly, due to the high mass flux of the combustion products. If the temperature profile reaches a high value (close to 500K), where generally the strength of aluminum alloy rapidly decreases, there will be a reduction in the load-bearing capacity of the wall, compromising the thruster's function.
2. During the operation time, internal walls of a thruster accumulate heat, which will be conducted through structure, during the time. This heat transfer can potentially cause an auto-ignition of the neighboring thrusters.

With a distance of 3 mm separating two adjacent thrusters, and which represents the calculated thickness a combustion chamber wall for one thruster, analyses of the heat transfer within the control block during the time activation of one thruster is conducted. To this end, to determine the thermal endurance limit of the selected structure, the three described thrusters are analyzed using a complex unsteady CFD and heat transfer simulations.

4.1. Input parameters of simulation

The simulation model of the combustion products flow and the heat transfer consists of:

- The thruster's fluid and the solid domain geometry as represented in fig. 7;
- The internal ballistic operating regime;
- Thermo-physical characteristics of combustion products [21] given in fig. 8;
- Thermo-physical characteristics of case and nozzle materials given in fig. 9 (experimentally determined);
- Turbulent characteristics of the internal flow.

For the simulation, a 2D axisymmetric geometry model is created for each motor, with the same case and different propellant grain and nozzle. The models are divided into 3 zones. The fluid domain corresponding to the combustion products flow space, and the solid regions corresponding to the motor case, nozzle and throat insert. The turbulence of the combustion products flow is calculated using the RNG k-ε turbulence model, while the flow within the boundary layer is modeled using scalable wall functions. A hybrid mesh is generated for all thruster models. Adaptation technique is used to achieve uniform y+ distribution (near 10) in boundary layer zones for accurate capturing heat transfer process, regarding Fluent User's Guide [22]. A convergence study was performed to assess the accuracy of the results, testing different mesh densities. The mesh elements are sized to accurately capture flow and heat transfer characteristics, with a total of around 300,000 elements for each thruster model.

Boundary conditions are defined by the internal ballistic parameters and the combustion characteristics of the propellant, which are provided in tab. 4.

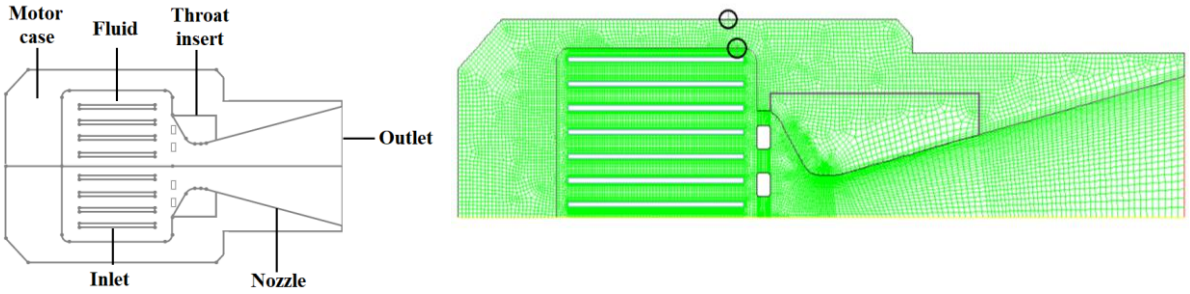

(a) (b)

Figure 7. Simulation model: (a) structure diagram and (b) grid diagram

Table 4. Boundary conditions

Parameter	Value	
Products mass flow rate [kgs^{-1}]	Motor 1	0.2473
	Motor 2	0.3879
	Motor 3	0.5366

Parameter	Inlet	Outlet
Pressure [Pa]	$200 \cdot 10^5$	$1 \cdot 10^5$
Temperature [K]	2350	300
Turbulence intensity [%]	5	5
Hydraulic diameter [m]	0.024	0.03

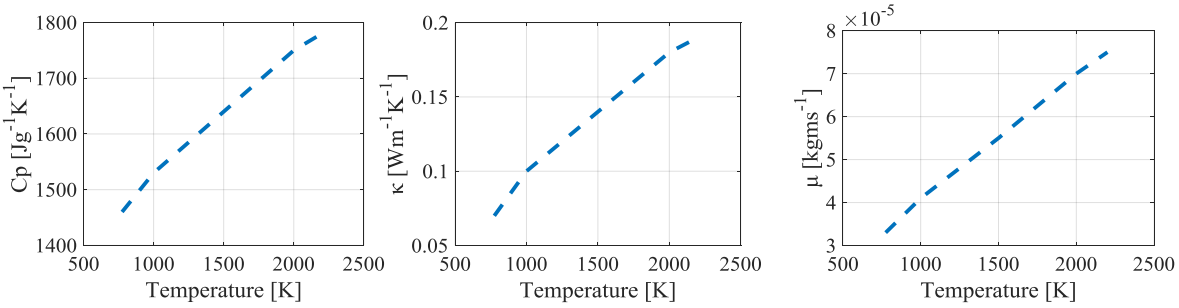

(a) (b) (c)

Figure 8. Thermo-physical characteristics of the combustion products:
(a) specific heat capacity, (b) thermal conductivity and (c) dynamic viscosity

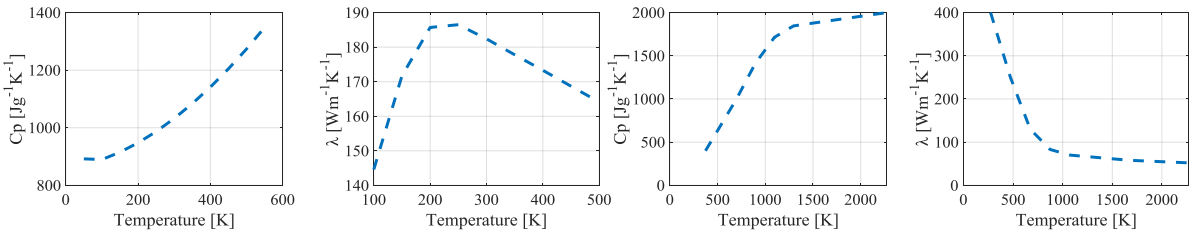

(a) (b)

Figure 9. Thermo- physical characteristics, specific heat and thermal conductivity of:
(a) aluminum alloy 7050 and (b) high density graphite

4.2. Simulations results

To conduct simulations, the commercial software FLUENT is selected. Using this software and the CFD models, it is possible to determine the temperature distribution contours, as well as, to extract temperature changes in time for any specified point. Two characteristics points are chosen and are fixed on: the internal and external wall as shown in fig. 7(b). Figure. 10 represents the temperature contour of each motor at t=11ms (at the end of the operating time).

Simulation results show that even for fast burning process, the motor casing is significantly heated. During thruster operating time, the heat propagates through the motor case and the wall temperature increases along the thickness. Comparing all motors, the third motor shows the greatest heat propagation since it has the highest products mass flow. According to temperature field, the maximum stress occurs at the nozzle throat. High temperatures are reached for the inner wall and the nozzle throat comparing to the outer wall, this is due to direct contact between these zones and the combustion gases, while the outer wall receives heat only by conduction through the walls material.

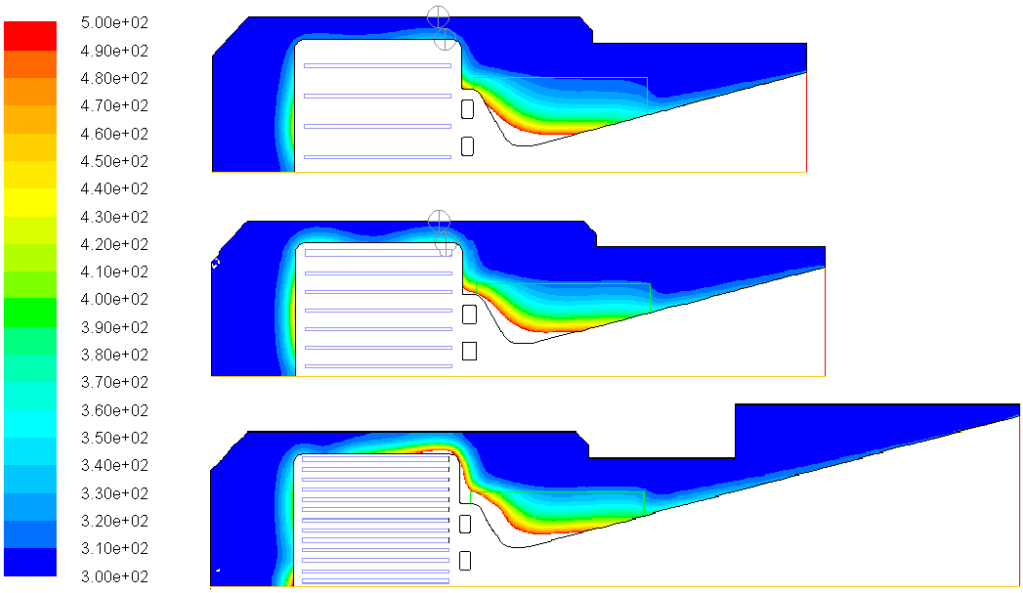

Figure 10. Temperature distribution at t =11 ms for: Motor 1 (above), Motor 2 (middle) and Motor 3 (below)

For a calculation step of 1 ms, temperature change in two selected characteristics points (inner and outer wall of case, shown in fig. 10), for each motor is given in fig. 11.

For the Motor 1 and Motor 2, the inner wall temperature at t=11ms rises from 300K up to 332K and 371K and then decreases to 311K and 319K respectively at t=150ms. Outer wall temperature rises from 300K to 303K and 307K at t=11ms, then keep rising to reach 310K and 321K respectively at t=33ms then start to decrease until equilibrium at 300K. These reached temperatures are far from the material strength loss temperature (≈500K) or the melting point of the aluminum alloy (≈750K). From a thermal perspective, Motor 1 and 2 are suitable for use.

On another side, for the Motor 3 the inner wall temperature rises from 300K to 548K at t=11ms, which is higher than the temperature of load-bearing capacity of the wall. The outer wall temperature rises from 300K to 325K at t=11ms, and then keep rising up to 374K at t=35ms. These temperature

values pose a potential risk to the reliability of the thruster's function, indicating that the configuration of Motor 3 is critical concerning the thermal durability of the applied material and thruster design.

Because of the significant thermal load in the nozzle throat, which is about 1000 K for all Motor models (for Motor 3 is above 1100), this part of the motor (nozzle throat) must be made from a more temperature-resistant material, such as high-density graphite.

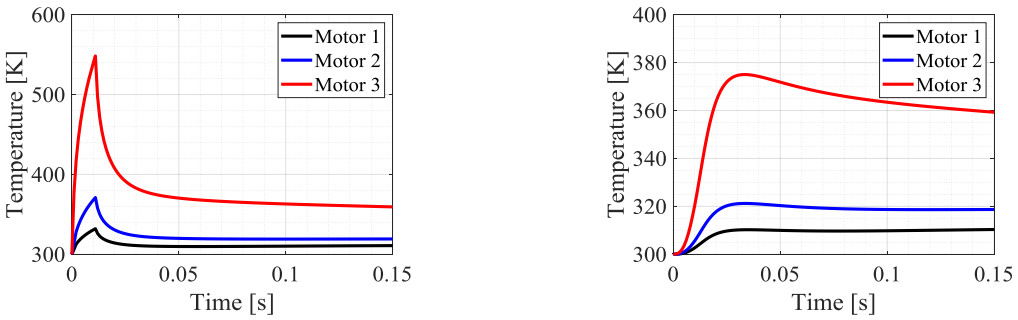

Figure 11. Temperature variation of characteristic points: (a) Inner wall and (b) Outer wall

5. Conclusion

In this paper, design and thermal analysis of impulse thrusters for control systems of guided missiles is investigated. Using the unsteady internal ballistic mathematical model, three models of thrusters were designed with identical casing and different nozzles and propellant grains. Prototypes of these motors and spiral shaped propellant grains were constructed, then tested on a static test bench. The good agreement between the experimental results, and the calculation predictions validates the mathematical model and demonstrates its use possibility for further impulse thrusters design.

Spiral-shaped propellants, thanks to their high surface burning area, show a high burn rate and very short operating time, what is sought in impulse thrusters. They also have a nearly neutral thrust force, what makes them favorable to use, and suitable for control systems application. Manufacturing irregularities of the propellant grain may influence the thruster's operational time, the shape of the thrust-time curve, and, consequently, its overall performance.

Thermal analysis demonstrated that, even for very short operating time of impulse thrusters, the heat transfer occurs, making it necessary and essential to consider thermal loads in their design. Aluminum alloys, due to their high strength to weight ratio, can be used to construct control block of missiles, while also minimizing its weight and cost comparing to other materials.

The designed and researched thruster models indicate that there is a critical amount of propellant material within the given thruster geometry at which thermal overload of the applied material occurs. If the system requires a higher mass flow rate within this geometry, modifications to the solution are necessary, either by employing thermal insulation or using thermally resistant materials.

Nozzle throat always represents the most sensitive zone to thermal stresses, based on this, they always should be constructed using thermally resistant materials.

The study highlights the importance of material selection, thermal analysis, and propellant design for optimizing impulse thruster performance and ensuring the reliability of control systems of missiles. Incorporating impulse thrusters into missile control systems represents a significant advancement. Future work could involve validation of thermal simulations through experimental

methods, using thermocouples or infrared cameras to measure temperatures at key thruster locations. Additionally, the design of a more compact missile control block could be explored, either by using spherical thrusters or reducing thruster length, which would result in lighter and more efficient missile control systems.

Nomenclature

A_b	-	Burning surface area, [m^2]	r	-	Burning rate, [ms^{-1}]
A_t	-	Nozzle throat area, [m^2]	T_c	-	Temperature of combustion, [K]
C_F	-	Thrust coefficient, [-]	t	-	Time, [s]
C_p	-	Specific heat capacity, [$JK^{-1}.kg^{-1}$]	V_c	-	Free volume in the combustion chamber, [m^3]
F	-	Thrust force, [N]	x	-	Burned web thickness, [m]
h	-	Spiral thickness, [m]	*Greek symbols*		
L	-	Spiral length, [m]	κ	-	Specific heat ratio, [-]
l	-	Spiral width, [m]	ρ_p	-	Propellant density, [kgm^{-3}]
p_c	-	Chamber pressure, [Pa]	λ	-	Thermal conductivity [$Wm^{-1}K^{-1}$]
R	-	Gas constant, [$Jkg^{-1}K^{-1}$]	μ	-	Dynamic viscosity, [$kgms^{-1}$]

References

[1] Karthikeyan, T. V., Kapoor, A. K., *Guided Missiles*, Defence Research & Development Organization, Delhi, 1990.

[2] Palumbo, N. F., Guest Editor's Introduction: Homing Missile Guidance and Control, *Johns Hopkins APL Technical Digest*, 29(2010), 1, p. 8

[3] Gupta, S.K., *et al*., Trajectory Correction Flight Control System using Pulsejet on an Artillery Rocket, *Defence Science Journal*, 58(2008), 1, pp.15-33

[4] Głębocki, R., Jacewicz, M., Sensitivity Analysis and Flight Tests Results for a Vertical Cold Launch Missile System, *Aerospace*, 7(2020), 168

[5] Bagley, C. J., General Dynamics Corp, Lateral thruster for missiles. Patent 4,967,982, 06 Nov 1990, https://patentimages.storage.googleapis.com/43/02/e2/02235cbc360569/US4967982.pdf

[6] Pavković, B., *et al*., Enhancing the Precision of Artillery Rockets Using Pulsejet Control Systems with Active Damping, *Scientific Technical Review*, 62 (2012), 2, pp. 10-19

[7] ***, Oryx, https://www.oryxspioenkop.com/2021/05/novel-capabilities-ukraines-vilkha-mrl.html?m=1

[8] Živković, S., *Technical Solutions and Gasodynamic Efficiency of Thrust Vector Control Systems for Missiles (in Serbian language)*, MTI, Belgrade, 2015

[9] ***, Zespol Badan Analiz Militarnych, https://zbiam.pl/kb-lucz-pokazalo-pocisk-rakietowy-wilcha/

[10] ***, Wikimedia, https://upload.wikimedia.org/wikipedia/commons/b/bd/JASDF_MIM-104_Patriot_PAC-3_Missile%28dummy_model%29_left_front_low-angle_view_at_Hamamatsu_Air_Base_October_20%2C_2019.jpg

[11] ***, Wikimedia, https://upload.wikimedia.org/wikipedia/commons/6/69/JASDF_MIM-104_Patriot_PAC-3_Missile%28dummy_model%29_seeker_%26_guidance_section_at_Hamamatsu_Air_Base_October_20 % 2C_2019.jpg

[12] Zečević, B., *et al*., Specific Design Features of Solid Propellant Rocket Motors for Shoulder-Launched Weapon Systems, *Proceedings*, 8th International Armament Conference on ,, Scientific Aspects of Armament and Safety Technology", Pultusk, Poland, 6-8 October, 2010

[13] Divac, S., Elements of Solid Propellants Rocket Motors Construction, in: *Solid Propellant Rocket Motors* (in Serbian language), MTI, Belgrade, 2013, pp 223-280

[14] Caveny. L. H., Summerfield, M., Micro-Rocket Impulsive Thrusters, Department of Aerospace and Mechanical Sciences, Princeton University, New Jersey, November 1971

[15] Platzek, H., Preliminary Solid Rocket Motor Design Techniques, Naval Weapons Center, China Lake, California, 1975.

[16] Živković, S., *et al*., Experimental Determination of Rocket Motor Internal Ballistic Coefficients and Performance Parameters, *Proceedings*, OTEH 2014: 6th International Scientific Conference on Defensive Technologies, Belgrade, Serbia, 2014, pp. 289-295

[17] Živković, S., *et al*, Solid Propellant Rocket Motor Components Initial Design, *Proceedings*, OTEH 2011: 4th International Scientific Conference on Defensive Technologies, Belgrade, Serbia, 2011

[18] Marjanović, G., *et al*., Program "SVOD" for Solid Propellant Grain Design, *Proceedings*, OTEH 2012: 5th International Scientific Conference on Defensive Technologies, Belgrade, Serbia, 2012

[19] Wolszakiewicz, T., *et al*., Thermochemistry of the Binary System Nitrocellulose+2,4-Dinitrotoluene, *Journal of Thermal Analysis and Calorimetry*. 77(2004), 353–361
[20] Alazeezi, M., *et al*., Two-Component Propellant Grain for Rocket Motor Combustion Analysis and Geometric Optimization, *Thermal Science*, vol. 26 (2022), 2B, pp. 1567-1578
[21] Živković, S., *et al*., Experimental and Simulation Testing of Thermal Loading in The Jet Tabs of a Thrust Vector Control System, *Thermal Science*, vol. 20 (2016), 1, pp. S275-S286
[22] ***, ANSYS Inc, Fluent User's Guide, http://www.ansys.com

Submitted: 12.09.2024
Revised: 01.12.2024
Accepted: 07.12.2024